Characteristics of the subtropical tropopause region based on long-term highly resolved sonde records over Tenerife

Juan J. Rodriguez-Franco[1] and Emilio Cuevas[1]

Received 30 March 2013; revised 10 September 2013; accepted 12 September 2013; published 2 October 2013.

[1] This study examines the structure of the subtropical tropopause region over Tenerife (the Canary Islands, Spain; 28°N, 16°W) based on a 20 year (1992–2011) ozonesonde data and European Center for Medium-Range Weather Forecasts ERA-Interim potential vorticity (PV) and zonal wind speed reanalysis. High-resolution vertical profiles allowed a detailed description of the subtropical tropopause break and the associated subtropical jet stream (STJ), where models fail to properly simulate the upper troposphere–lower stratosphere (UTLS). The subtropical UTLS is revealed as a complex atmospheric region with a thickness ∼8 km, which is examined through the analysis and evaluation of four different tropopause definitions: thermal (TT), cold point, ozone (OT), and dynamical (DT) tropopauses. A novel method to determine the DT based on the vertical gradient of Lait's modified PV is presented and the concept of a second DT has been introduced for the first time. Monthly climatologies of tropopause height and potential temperature are calculated for double and single tropopause events. The 14.3 km height level is used to differentiate between tropical and extratropical UTLS regimes, intimately linked to the position of the STJ. There is fairly good consistency between all the defined tropopauses under the double tropopause scheme, except in spring, when the OT is observed at lower levels due to frequent baroclinic instabilities in the upper troposphere. As concerns to single tropopause events, the same pattern is found from April to June, reflecting the influence of analogous processes during these months. In winter, altitude differences between OT, DT, and TT resulted from poleward STJ excursions forced by blocking systems over the North Atlantic. Analysis of the tropopause inversion layer showed distinctive features for tropical and midlatitude tropopauses.

Citation: Rodriguez-Franco, J. J., and E. Cuevas (2013), Characteristics of the subtropical tropopause region based on long-term highly-resolved sonde records over Tenerife, *J. Geophys. Res. Atmos.*, *118*, 10,754–10,769, doi:10.1002/jgrd.50839.

1. Introduction

[2] Over the past two decades, there has been growing interest in the tropopause region among the atmospheric scientific community. It is now broadly accepted that the tropopause plays a key role in a variety of topics. They include concerns about correlation between tropopause height and stratospheric ozone changes [*Steinbrecht et al.*, 1998; *Varotsos et al.*, 2004], stratosphere-troposphere exchange (STE) of chemical species [*Danielsen*, 1968; *Holton et al.*, 1995; *Pan et al.*, 2004] and tropopause as a sensitive indicator of anthropogenic-induced climate change [*Santer et al.*, 2003; *Sausen and Santer*, 2003], among others.

[3] The existence of the tropopause was discovered during the late nineteenth and early twentieth centuries thanks to observations made simultaneously by Leon Teisserenc de Bort in France [*Teisserenc de Bort*, 1902] and Richard Assmann in Germany [*Assmann*, 1902]. For an extensive review of the history of tropopause discovery as well as of early studies of the tropopause during the last century, see *Hoinka* [1997]. Although the tropopause was discovered more than a hundred years ago, some aspects of the mechanism responsible for this narrow atmospheric region remain unclear. Most of the efforts to investigate the tropopause nature had focused on some of the relevant mechanisms involved, e.g., radiative processes and baroclinic dynamics [*Thuburn and Craig*, 1997; *Haynes et al.*, 2001; *Schneider*, 2004].

[4] From a broad perspective, the tropopause has conventionally been defined as the boundary between the troposphere and stratosphere, often characterized by an abrupt change in physical and chemical parameters [e.g., *Holton et al.*, 1995, and references therein]. Because of the incomplete knowledge of this atmospheric region, a variety of tropopause definitions based on this feature have been proposed. The conventional tropopause definition is based on the temperature lapse rate, which relates directly to the static stability of the atmosphere [*World Meteorological*

[1]Izaña Atmospheric Research Center, AEMET, Santa Cruz de Tenerife, Spain.

Corresponding author: J. J. Rodriguez-Franco, Izaña Atmospheric Research Center, AEMET, La Marina 20, 6 Planta, ES-38071 Santa Cruz de Tenerife, Spain. (jurodriguezf@aemet.es)

2169-897X/13/10.1002/jgrd.50839

Organization (WMO), 1957]. We will refer to this type of tropopause as the thermal tropopause. Sometimes, especially in the tropics, the cold point tropopause has been used in terms of the coldest point in the vertical temperature profile, mostly related to the transport of water vapor through the tropopause [*Holton et al.*, 1995; *Highwood and Hoskins*, 1998; *Zhou et al.*, 2001; *Fueglistaler et al.*, 2009]. Additionally, the 100 hPa level has been commonly used as a surrogate for the tropical tropopause [e.g., *Mote et al.*, 1996]. Nevertheless, previous studies have documented this as a poor approximation to the tropical tropopause [*Seidel et al.*, 2001]. The tropopause can also be defined in terms of the isentropic Ertel's potential vorticity, PV (the standard potential vorticity unit being defined as 1 PVU = 10^{-6} m^2 s^{-1} K kg^{-1}), referred to hereafter as the dynamical tropopause [*Reed*, 1955; *Danielsen*, 1968; *Shapiro*, 1978; *Holton et al.*, 1995]. The advantage of the dynamical tropopause resides mainly in the conservative nature of PV under adiabatic, frictionless conditions, which makes the PV surface defined adequate for STE processes analysis. Unfortunately, a variety of PV values ranging from 1 to 4 PVU for determining the dynamical tropopause has been proposed [*Danielsen*, 1968; *Hoerling et al.*, 1991; *Hoinka*, 1998]. In addition to the temperature lapse rate and potential vorticity, chemical tracers such as ozone have also been used to identify the tropopause. *Bethan et al.* [1996] proposed a set of criteria to determine the tropopause level from ozone profiles using both the ozone mixing ratio and the ozone mixing ratio vertical gradients. We will refer to this tropopause as the ozonopause. A shortcoming of the ozonopause arises from the fact that the choice of the actual ozone threshold value used in the determination of the tropopause level is not well known. For this reason, a new characterization of the chemical change at the tropopause based on tracer-tracer correlations between stratospheric and tropospheric species has been proposed [*Hoor et al.*, 2002; *Zahn et al.*, 2004; *Pan et al.*, 2004; *Kunz et al.*, 2009].

[5] Most of the studies about the tropopause within the last decade have focused mainly on three distinct aspects of this narrow atmospheric region: (1) analysis of multiple tropopause systems [*Schmidt et al.*, 2006; *Randel et al.*, 2007; *Añel et al.*, 2007; *Peevey et al.*, 2012], (2) the tropopause as a chemical transport barrier [*Hoor et al.*, 2002; *Pan et al.*, 2004; *Hegglin et al.*, 2009; *Kunz et al.*, 2011b], and (3) detailed analysis of the thermodynamic properties of the tropopause region [*Birner*, 2006; *Randel et al.*, 2007; *Bell and Geller*, 2008; *Schmidt et al.*, 2010; *Son et al.*, 2011]. As a result of these efforts, there has been a notable improvement in our physical understanding of the tropopause region [e.g., *Gettelman et al.*, 2011].

[6] It is well known that globally the tropopause is not homogenous but reaches the highest altitude at tropics and decreases toward the poles [*Rex*, 1969]. It is also acknowledged that the transition from the high tropical tropopause to the lower midlatitudes tropopause is not continuous but presents some sharp discontinuities, especially at subtropical latitudes [*Kochanski*, 1955; *Randel et al.*, 2007; *Pan et al.*, 2009]. Although multiple tropopause systems were known to exist since the middle of the last century, it was not until the last decade that considerable efforts have been made to investigate these types of structures. Traditionally, it has been common to associate multiple tropopause events with tropopause folding caused by deep lows, cutoff lows, and tropospheric frontal systems [*Shapiro*, 1978; *Keyser and Shapiro*, 1986]. *Randel et al.* [2007], owing to the absence of any clear zonal structure of global multiple tropopause events, suggested that they are caused by dynamical processes other than tropopause folding. *Schmidt et al.* [2006], based on GPS radio occultation measurements, and later *Randel et al.* [2007], based on radiosondes, GPS radio occultation measurements, and ERA40 reanalysis, developed a global climatology of multiple thermal tropopauses systems, concluding that they are a usual feature for the 30°–50° zonal band during winter and spring for both hemispheres, with a maximum occurrence near the subtropical jet stream (STJ). Similar results were found simultaneously by *Añel et al.* [2007] based on IGRA (Integrated Global Radiosonde Archive). More recently, *Peevey et al.* [2012] have documented similar results using 3 years (2005–2007) of high-resolution dynamics limb sounder (HIRDLS) data. Although the formation and maintenance of multiple tropopause system are still not completely understood, increasing evidence points to Rossby wave dynamics as playing an important role in the occurrence of multiple tropopauses [*Pan et al.*, 2009; *Castanheira and Gimeno*, 2011; *Castanheira et al.*, 2012; *Peevey et al.*, 2012].

[7] The classical "thinking" of the tropopause as a sharp boundary has been replaced by a more meaningful and realistic conception. In this new scheme, the tropopause is understood as a transition region of finite depth between the troposphere and the stratosphere with mixed characteristics of both spheres. Although not a new finding [e.g., *Atticks and Robinson*, 1983], the increasing number of airborne tracer measurements near the tropopause over the last decade have allowed great advances in the characterization of this transition layer referred to as the extratropical tropopause transition layer for midlatitudes [*Hoor et al.*, 2002; *Pan et al.*, 2004; *Zahn et al.*, 2004; *Hegglin et al.*, 2009] and the tropical tropopause transition layer (TTL) in the tropics [*Gettelman and Forster*, 2002; *Gettelman and Birner*, 2007; *Fueglistaler et al.*, 2009].

[8] Further improvement of our knowledge of the tropopause is related to a narrow layer of very high static stability just above both the tropical and the extratropical tropopauses, currently known as the tropopause inversion layer (TIL) [*Birner et al.*, 2002; *Birner*, 2006]. It is not clear which mechanisms contribute to the development and maintenance of the TIL, but both radiative [*Randel et al.*, 2007; *Kunz et al.*, 2009] and dynamic [*Wirth*, 2003, 2004; *Birner*, 2006, 2010; *Son and Polvani*, 2007] processes may be involved. Other studies have revealed a strong connection between the TIL and the tropopause transition layer [*Randel et al.*, 2007; *Hegglin et al.*, 2009; *Kunz et al.*, 2009].

[9] Model analyses provide a global picture of the tropopause. However, they are not able to adequately resolve the observed fine structures of the tropopause region because of their lower vertical resolution. This is especially true in subtropical latitudes, where multiple or layered thermal tropopause is likely to be found [*Reichler et al.*, 2003; *Bell and Geller*, 2008; *Homeyer et al.*, 2010; *Son et al.*, 2011]. The Izaña Atmospheric Research center (Tenerife, the Canary Islands, Spain; 28°N, 16°W) contributes to the Network for the Detection of Atmospheric Composition Change (NDACC) with four remote sensing program

(electrochemical concentration cell (ECC) sonde, Brewer spectrophotometer, differential optical absorption spectroscopy, and Fourier transform infrared). The application of inversion techniques to derive column amounts of different chemical components in the troposphere and the stratosphere needs accurate information of the tropopause level, which is a challenging problem because the Canary Islands are located just below the descending branch of the Hadley cell, characterized by a frequent presence of the STJ and the associated transition between the tropical tropopause and the midlatitude tropopause. On the other hand, the precise determination of atmospheric components trends in the upper troposphere and lower stratosphere (UTLS) requires a precise knowledge of the vertical structure of the tropopause region and its variation over the year, in order to properly choose the altitude levels of the corresponding atmospheric component long-term series.

[10] The main motivation of this work is to improve our knowledge of the tropopause region in the subtropics through a joint analysis of 20 year radiosonde data of ozone and temperature, complemented with potential vorticity vertical profiles and latitude-height cross sections of zonal wind from the European Center for Medium-Range Weather Forecasts (ECMWF) ERA-Interim analysis. Long-term vertical profiles, in which we have based our study, constitute a very valuable data set because it allows us to identify fine-scale structures in the subtropical UTLS and characterize them with climatological value. In particular, we focus on the occurrence of double tropopause systems and their relation with the presence of the STJ. Tropopauses calculated from different definitions are used to check their consistency in the subtropical region and for assessing their similarities and differences in terms of the position of the STJ and meridional transport processes in the UTLS. A new method for determining the dynamical tropopause based on vertical gradient of Lait's modified potential vorticity has been implemented. The concept of a second dynamical tropopause has been introduced and analyzed in this paper. We also explore the fine-scale structure of the tropopause region, focusing on the seasonal cycle of the extratropical and tropical tropopause inversion layer.

[11] The paper is organized as follows. In section 2 the observations and data processing are described, introducing the different tropopause definitions used. Results are shown in section 3 including the following subsections: single and multiple thermal tropopause frequency distributions and its relation with the STJ (section 3.1), tropopause height and potential temperature seasonal cycle using four different tropopause definitions (section 3.2), and finally a statistical analysis of the tropopause inversion layer for the subtropical thermal tropopause (section 3.3) are discussed. Summary and concluding remarks are found in section 4.

2. Data and Methods

2.1. Data Description

[12] Data from the Izaña Atmospheric Research Center (CIAI-AEMET; 28°N, 16°W; http://izana.aemet.es) ozonesonde program are used in this work to obtain a climatology of the subtropical UTLS region. The ozonesounding program at Tenerife station was initiated in November 1992 with observations being made on a weekly basis [*Cuevas et al.*, 1994], except for some field campaigns in summer when additional ozonesondes were launched. This program is part of the Global Atmospheric Watch and NDACC.

[13] The operational sensor at CIAI ozonesonde station is the electrochemical concentration cell (ECC) for ozone [*Komhyr*, 1969], coupled to a Vaisala RS80 radiosonde until 2002, and to a Vaisala RS92 radiosonde afterward, for temperature, pressure, and humidity retrievals. Wind speed and direction are measured by GPS. Given the typical ascent rate of the radiosonde balloon of 5 m s^{-1}, this results in an average vertical resolution for raw data of ∼30 m for temperature, ∼100–150 m for ozone, and ∼150 m for wind measurements. We remove outliers by applying to individual profiles the algorithm described by *Chawla and Sun* [2006], then interpolating all the variables at 100 m intervals by applying the spline interpolation technique. This procedure substantially reduces the observed noise in vertical profiles, due mainly to sensor performance.

[14] A total number of 1090 high-resolution vertical profiles have been analyzed, covering a period of 20 years, from November 1992 to December 2011. In order to compute an annual climatology, we considered only those profiles that reached, at least, 20 km height. Additionally, only profiles for which the tropopause algorithm succeeded in assigning a proper tropopause level were selected (see below the World Meteorological Organization (WMO) algorithm description). This resulted in a total of 1016 ozonesonde profiles (∼6% of the profiles were rejected), distributed in 80–90 profiles per month, except for July, when a greater number of soundings are available (∼145). Balloons typically reach maximum altitudes well above 25 km (∼ 96% of ozonesondes), higher than the upper limit of the region of interest in the present study, ∼20 km (∼ 99.8% of ozonesondes).

2.2. Tropopause Definitions

[15] The different tropopause definitions used in this work together with the algorithms employed to determine their level heights are presented. We can consider these empirical definitions as incomplete by nature, since each of them is primarily based on isolated properties of the tropopause level. Therefore, a multi-approach analysis of the UTLS using all the defined tropopauses will allow a more comprehensive characterization of this region in the subtropics.

2.2.1. Thermal Tropopause

[16] In this work we will refer to the tropopause identified using the formal lapse rate definition [*World Meteorological Organization (WMO)*, 1957] as the thermal tropopause (TT): *"The first lapse rate tropopause is defined as the lowest level at which the lapse rate decreases to 2 K/km or less, provided that the averaged lapse rate between this level and all higher levels within 2 km does not exceed 2 K/km. If above the first tropopause, the average lapse rate between any level and all higher levels within 1 km exceeds 3 K/km, then a second tropopause is defined by the same criterion as for the first tropopause. This tropopause may be either within or above the 1 km layer."*

[17] The WMO algorithm accounts also for multiple tropopause occurrence, in which case we will denote the first, second, and third thermal tropopause as TT1, TT2, and TT3, respectively. When a single thermal tropopause is detected, it will be referred to as SingT. We have rejected

tropopause levels corresponding to $P > 500$ hPa in order to avoid including tropospheric thermal inversions related to subsidence or baroclinic processes into the statistics. Additionally, we have discarded TT2 in multiple tropopause events whenever the height difference between TT1 and TT2 levels was lower than 1.5 km.

2.2.2. Cold Point Tropopause

[18] The Cold Point Tropopause (CPT) is located at the minimum temperature level found in the transition region between the troposphere and the stratosphere [*Highwood and Hoskins*, 1998]. Although the CPT is physically meaningful only in the tropics, often related to studies of cross-tropopause flux of water vapor [*Holton et al.*, 1995], we include it in this work because the subtropics are transition regions from tropics to midlatitudes.

2.2.3. Ozonopause

[19] Following *Bethan et al.* [1996], we have defined the ozonopause (OT) as the lowest altitude where the following three criteria are met:

[20] 1. Vertical gradient (evaluated over a depth of ∼200 m) in ozone mixing ratio exceeds 60 ppbv/km.

[21] 2. Ozone mixing ratio greater than 80 ppbv.

[22] 3. Mixing ratio immediately above the tropopause exceeds 110 ppbv. This criterion rejects layers of stratospheric air in the troposphere where the maximum mixing ratio is less than 110 ppbv.

[23] A minor modification to this definition has been done in this work, replacing criterion 3 with the following: "The averaged mixing ratio within 1.5 km immediately above the tropopause exceeds 110 ppbv". We have found, through a detailed inspection of vertical profiles, that this modification optimizes the algorithm, discarding ozone-rich stratospheric air layers (with a typical thickness of 1.5 km) into the upper troposphere [*Kahya et al.*, 2005]. Otherwise, small changes in the threshold values of ozone mixing ratio and ozone vertical gradients are not likely to be critical in determining the ozonopause height [*Sivakumar et al.*, 2006].

2.2.4. Dynamical Tropopause

[24] The tropopause can also be defined in terms of the isentropic Ertel's potential vorticity (EPV) as introduced by *Rossby* [1940] and *Ertel* [1942]. Under the hydrostatic approximation, the EPV can be expressed in terms of the static stability $N^2 = \frac{g}{\theta}\frac{\partial\theta}{\partial z}$, where θ is the potential temperature and g is the acceleration of gravity, as

$$\mathrm{EPV} = N^2 \frac{\theta}{\rho g}(\zeta_\theta + f) \tag{1}$$

[25] Here ζ_θ is the relative vorticity evaluated on isentropic surfaces, f is the Coriolis parameter, and ρ is density [e.g., *Gettelman et al.*, 2011]. It follows from equation (1) that EPV contains both dynamic and thermodynamic properties. In particular, EPV is proportional to the static stability. Given that a jump in static stability at the TT level is expected, there will be a corresponding discontinuity in EPV at the same level. Following these considerations, we have defined the dynamical tropopause (DT) as the height level where a maximum value in potential vorticity vertical gradient is found. It is worth noting that despite the original concept of the DT was based on the isentropic gradient of EPV [*Reed*, 1955], no global determination of the DT based on this concept has been performed, with the exception of a recent work by *Kunz et al.* [2011a]. In this study the authors developed a novel method for determining the global DT which involves both isentropic gradient of EPV and horizontal wind field. The method we use in the present work is substantially different (and, not least, easier to implement) since we determine the DT level dependent on the maximum potential vorticity gradient with altitude levels.

[26] Ertel's potential vorticity has been obtained from the ECMWF ERA-Interim reanalysis data set; analyses of temperature and wind fields at standard levels from 1000 hPa to 10 hPa have been used to compute EPV vertical profiles for each day with ozonesonde data and finally interpolating them to 100 m vertical resolution levels. We restrict the analyses to 12:00 UTC, the nearest time to the ozonesonde launching.

[27] A problem arising from the definition of the EPV (equation (1)) is its exponential increase with altitude because ρ is a monotonic function of altitude. To avoid this shortcoming, we employed Lait's modified potential vorticity (LPV) [*Lait*, 1994], defined as the EPV multiplied by a scaling factor $(\frac{\theta}{\theta_0})^{-\frac{9}{2}}$, where θ_0 is a constant to make the scaling factor dimensionless. This scaling preserves both the unit and the conservation properties of the potential vorticity, maintaining its structure on any isentropic surface to within a constant multiplicative factor. For the calculus of LPV, we scale the EPV vertical profiles multiplying each level by the corresponding factor $(\frac{\theta}{375})^{-\frac{9}{2}}$.

[28] First, the LPV vertical gradient is computed by means of centered differences for all altitudes in a given profile, then applying a five-point (0.5 km) running average in order to reduce the noise in individual data. The DT level has been assigned to the altitude level corresponding to a maximum in the LPV vertical gradient profile from 6 km (which corresponds roughly to 500 hPa level) to 20 km height. Several upper bounds within the 20–25 km range have been checked, with no significant differences in the results. In the case of multiple thermal tropopause events, we applied an additional criterion to analyze the structure of the LPV vertical gradient in the vicinity of both the lower (TT1) and the higher (TT2) components. We proceed in this case as follows: First, we looked for a maximum in LPV vertical gradient from 6 km height to 2 km above the TT1 (we used this threshold by analogy with the WMO algorithm for the thermal tropopause). We then defined a second DT as the height level where a maximum in LPV vertical gradient was found from this point (2 km above the TT1) to 20 km height, far enough from the upper boundary of the tropical tropopause transition layer [*Gettelman and Forster*, 2002; *Gettelman and Birner*, 2007; *Fueglistaler et al.*, 2009]. Both first and second dynamical tropopauses will be referred to hereafter as DT1 and DT2, respectively. Note that the proposed approach may have difficulties in the near vicinity of jets, where PV isopleths distortions are expected to modify LPV vertical gradients. An example of vertical profiles of the parameters used in the detection of the DT, including the levels assigned to the thermal and the dynamical tropopauses, is shown in Figure 1 for single (bottom) and multiple (top) tropopause events.

2.3. Methodology of Tropopause Climatology

[29] In order to establish a climatology of different parameters associated with the tropopause region, we have

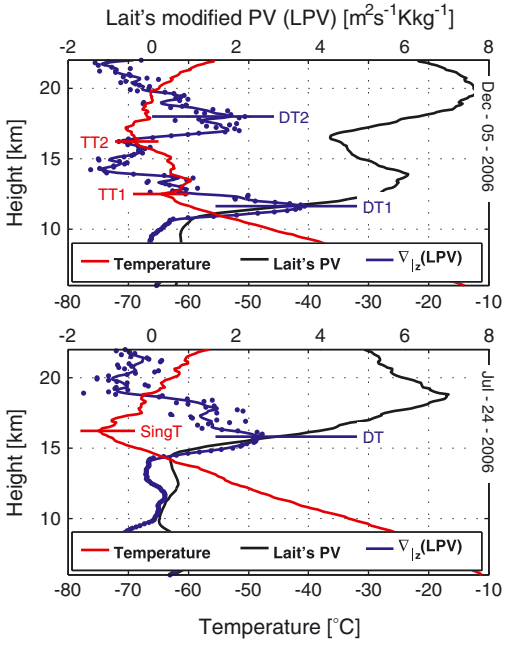

Figure 1. Vertical profiles of temperature (red line), Lait's modified PV (LPV, solid black line), and LPV vertical gradient (solid blue line) derived from radiosonde and ECMWF ERA-Interim potential vorticity for (top) multiple and (bottom) single tropopause events. The horizontal lines mark the location of thermal tropopauses, defined by the temperature lapse rate criterion, and dynamic tropopauses as defined by the PV gradient-based method.

assigned the first (or unique) TT level as the height reference. The use of a tropopause level-based vertical scale, as defined, allows to retain information relative to the tropopause region, filtering from long-term averages the smearing effect induced by the temporal variability of the tropopause height [*Logan*, 1999; *Birner et al.*, 2002; *Pan et al.*, 2004]. Once all the vertical profiles were referenced to the TT, we averaged all soundings in a given month for all years. As a measure of the statistical significance of the climatological means, we have used the expression SEM = $\sigma/\sqrt{n}$ as an approximation to the standard error of the mean, where σ is the standard deviation of the monthly means and n is the total number of profiles in a given month. Since the available number of soundings per month is very homogeneous, about 80–90 profiles, except for July, with a total number of 144, the same parameter provides also an estimation of the natural variability of the monthly means.

3. Results

3.1. Frequency Distribution of Subtropical Thermal Tropopauses

[30] Due to the thermal definition of tropopause, assuming a first-order discontinuity of temperature in the vertical, a discontinuity in air mass static stability at the tropopause level is expected. Vertical profiles of static stability as a function of the altitude relative to the first (or unique) thermal tropopause are shown in Figure 2. We have plotted two data sets representative of summer (June-August-September) and winter (January-February-March). Figure 2 shows that the TT level coincides with a sharp discontinuity in static stability, which, in turn, confirms that we have correctly identified the TT level.

[31] We have computed the seasonal cycle of TT occurrence frequency, grouping into single and multiple tropopause events classes all the available vertical profiles, according to the number of thermal tropopauses detected as stated by the WMO algorithm. Results are shown in Figure 3. Additionally, we have plotted the seasonal cycle of the wind speed, labeling 10, 20, and 30 m s^{-1} isotachs from 5 to 20 km height. Occurrence distributions include statistics for TT1, TT2, and TT3.

[32] Figure 3 suggests a strong relationship between the distribution of tropopause occurrence frequency and the STJ position relative to the station's latitude. To confirm this, we have developed a climatology of the STJ position by calculating monthly averages of the latitude-height cross sections of ECMWF ERA-Interim zonal wind for the period November 1992 to December 2011 and for the longitude of the station (16°W). Finally, we have grouped those months showing similar results for the STJ position in relation to the latitude of Tenerife (Figure 4).

[33] Around 80% of the vertical ozonesoundings show multiple thermal tropopauses during winter-early spring when a strong STJ is located south of Tenerife (see Figure 4). Decreasing frequency of double tropopause occurrence is observed from April to June, closely related to the annual migration of the STJ from south to north and, consequently, to the increasing frequency of cases when the STJ is observed northward of Tenerife [e.g., *Cuevas et al.*, 1999]. Note in Figure 4 that the STJ is practically over Tenerife in June. In summer the situation is quite different, with less than 5% of multiple tropopause occurrences. A weakened STJ is clearly observed north of Tenerife during this season, resulting in a typically tropical UTLS. In autumn a weak STJ is usually located south of Tenerife. It is not until November to December that more than 50% of multiple tropopause occurrences are observed, resembling the winter situation. These results are consistent with the knowledge that double tropopauses are preferably found at and poleward of the STJ

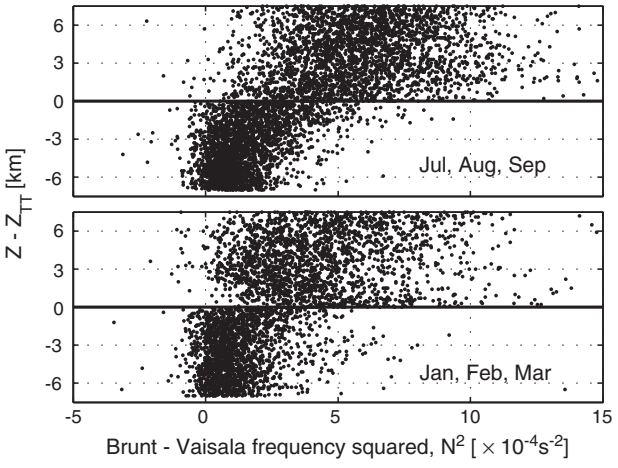

Figure 2. Buoyancy frequency squared (N^2) as a function of altitude relative to the first (or unique) thermal tropopause detected.

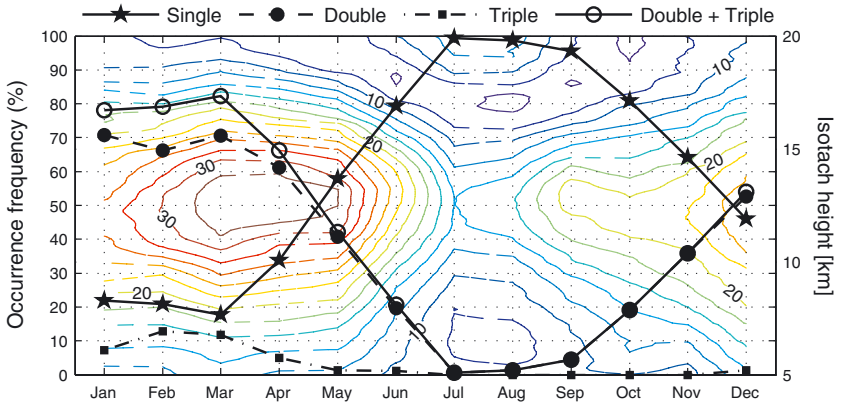

Figure 3. Seasonal cycle of single and multiple thermal tropopause occurrence frequency and wind speed over Tenerife derived from radiosondes data for the 1992–2011 period. Results are shown for single (solid stars with solid line), double (solid circles with dashed line), and triple (solid squares with dash-dotted line) tropopause events. Open circles with solid line denotes the sum of occurrence frequency for double and triple thermal tropopauses.

[*Castanheira and Gimeno*, 2011; *Peevey et al.*, 2012]. The higher frequency of triple tropopauses is registered between January and April when a strong STJ is located south of Tenerife. Triple tropopauses are not observed from June to November when the STJ is located over or north of Tenerife.

[34] We show in Figure 5 the distribution of the TT height derived for two samples representative of single (July-August-September) and multiple (January-February-March) thermal tropopause events (see also Figure 3). The winter period shows a bimodal structure with maximum occurrences in tropopause height at ∼16 km and at ∼12 km, both components being well separated from each other at ∼14.3 km. With respect to summer, it is characterized by a unimodal tropopause altitude distribution showing a single maximum centered at ∼16 km. Note the down-skewed distribution for both summer and winter lower components. Several studies [e.g., *Wirth*, 2001] have related large cyclonic vorticity associated with baroclinic disturbances in the UTLS with an increasing (decreasing) tropopause pressure (height). This provides an explanation for the anomalous low tropopause levels showed in both winter (<10 km) and summer (<14.3 km) statistics in Figure 5. The observed differences between both summer and winter higher components are also of interest. During winter, extremely high thermal tropopauses are detected. In contrast, the summer statistics present an abrupt cutoff at around 17.5 km, with very few tropopauses found above this level. The higher tail seen in winter statistics, not present during summer, may be mainly due to the presence of the STJ which acts as a disturbing force for the thermodynamical structure in its vicinity.

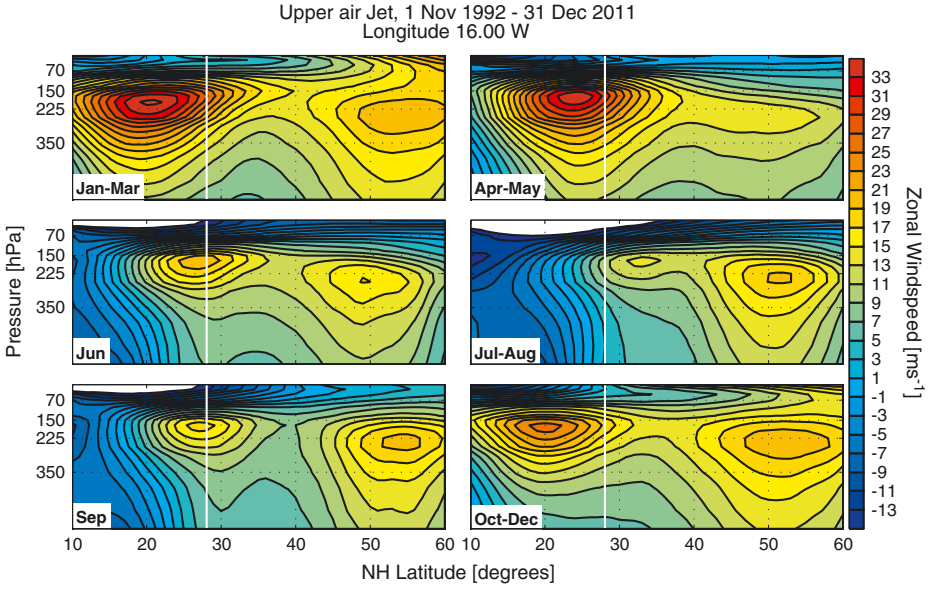

Figure 4. Averaged latitude-height cross sections (for 16°W) of ECMWF ERA-Interim zonal wind (m s^{-1}) for the period November 1992 to December 2011. Months were grouped into six time periods based on the position of the STJ relative to the station's latitude (marked with a vertical white line).

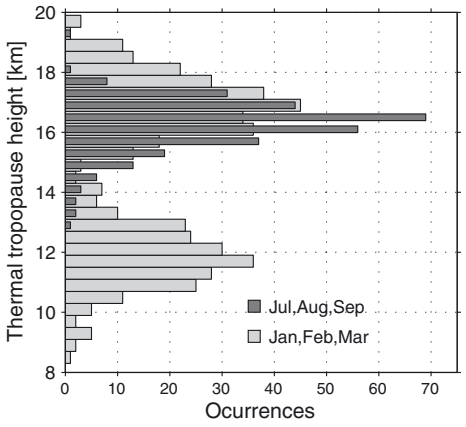

Figure 5. Frequency histogram of thermal tropopause height calculated for two samples representative of single (July, August, and September; dark grey) and multiple (January, February, and March; light grey) tropopause events.

As a result, multiple thermal tropopauses (more than two) are likely to be found.

[35] Table 1 shows a distribution analogous to Figure 5 but for all months separately, splitting the available profiles into multiple and single thermal tropopause, the latter being further split into two subgroups depending on whether the altitude of the tropopause level was higher or lower than 14.3 km. This value coincides with the altitude where a minimum in tropopause occurrences is observed in winter statistics, and where more than 95% of tropopause heights are found to be above it in summer statistics (see Figure 5). We use the 14.3 km height level as a threshold for classifying thermal tropopauses: Tropopause levels below 14.3 km will be considered as representative of midlatitudes, while tropopause levels higher than 14.3 km will be considered as tropical tropopauses. A similar threshold height has been used by several authors in discussing double tropopause climatology [*Randel et al.*, 2007] and trace gas distribution in the UTLS [*Pan et al.*, 2004].

3.2. Subtropical Tropopause Climatology

[36] Monthly mean tropopause height and potential temperature are discussed next for the four tropopause definitions used in this paper (TT, CPT, OT, and DT). A total of 1016 soundings is split into two subgroups depending on whether the temperature profiles showed single or multiple thermal tropopauses. When computing multiple thermal tropopauses statistics, we have omitted monthly means for which the occurrence frequency of double tropopauses was ≤15%. As regards to the TT3, we have omitted monthly means whenever the occurrence frequency of such events was ≤5%.

3.2.1. Subtropical Thermal and Cold Point Tropopauses

[37] The mean seasonal cycle of TT and CPT height and θ has been analyzed for multiple (Figure 6, left column) and single (Figure 6, right column) thermal tropopause events. For multiple thermal tropopauses, TT1 exhibits the higher amplitude for the seasonal cycle, ranging from a minimum height ∼12 km in winter to a maximum ∼13 km in late spring (Figure 6a). This winter to summer height transition occurs in a rather slow process from March to June, following the northward migration of the STJ in the vicinity of Tenerife. The TT2 height shows little seasonal variability, ∼16.5 km for all the months with occurrence frequencies >15%. Slightly higher values of TT2 height (∼17 km) are observed from April to June. These results are similar to the tropopause features observed in previous analysis of multiple tropopause systems [*Bischoff et al.*, 2007; *Randel et al.*, 2007]. The double tropopause thickness, defined here as the altitude difference between the TT1 and the TT2, is maximum in winter (∼5 km) and minimum in late spring (∼3 km), in agreement with a recent study by *Peevey et al.* [2012]. The annual cycle of tropopause θ is similar to that of height (Figure 6c). The values of θ_{TT1} and θ_{TT2} vary in the vicinity of 335 K and 400 K isentropic surfaces, respectively, with maximum (minimum) values during late spring (winter), ∼345 K (∼335 K) for TT1 and ∼415 K (∼400 K) for TT2. With respect to TT3, we found a frequency occurrence from 5% to ∼15% only during the period from January to April, with mean height around 18 km and very low variability. The CPT is on average up to ∼1 km higher than TT2, in agreement with previous studies [*Seidel et al.*, 2001; *Kishore et al.*, 2006; *Sivakumar et al.*, 2011]. Both CPT and TT3 are found at levels well close to each other. Maximum θ values are observed at the TT3 level during winter to early spring (∼425 K), quite similar to the values observed of θ_{CPT} during the same period.

[38] With respect to single thermal tropopause events (Figure 6, right column), we have discarded from the calculus those profiles for which SingT height was found to be ≤14.3 km. The number of these profiles is not statistically significant, except for November and December (see Table 1). Note that a single thermal tropopause higher than 14.3 km is observed between June and September in over 80% of cases, just in the period when the STJ is located above or north of Tenerife. This result confirms that the 14.3 km threshold is suitable to discriminate sample air masses with tropical characteristics from those with extratropical characteristics. Thereby, by selecting SingT heights > 14.3 km, we will refer to the tropical upper troposphere.

Table 1. Monthly Samples and Thermal Tropopause Distribution, Grouped as Double and Single Event[a]

	Jan	Feb	Mar	Apr	May	Jun	Jul	Aug	Sep	Oct	Nov	Dec
All	82	86	85	80	76	92	144	76	68	73	78	76
Double	**64**	**68**	**70**	**53**	32	19	1	1	3	14	28	**42**
Single	18	18	15	27	**44**	**73**	143	75	**65**	**59**	**50**	35
Single>14.3 km	9	13	14	15	27	62	**143**	**74**	55	47	30	16
Single≤14.3 km	9	5	1	12	17	11	0	1	10	12	20	19

[a]Single thermal tropopause is further split in two groups, depending on the height range (higher or lower than 14.3 km). Most frequent systems (double or single) are highlighted in bold-face for each month.

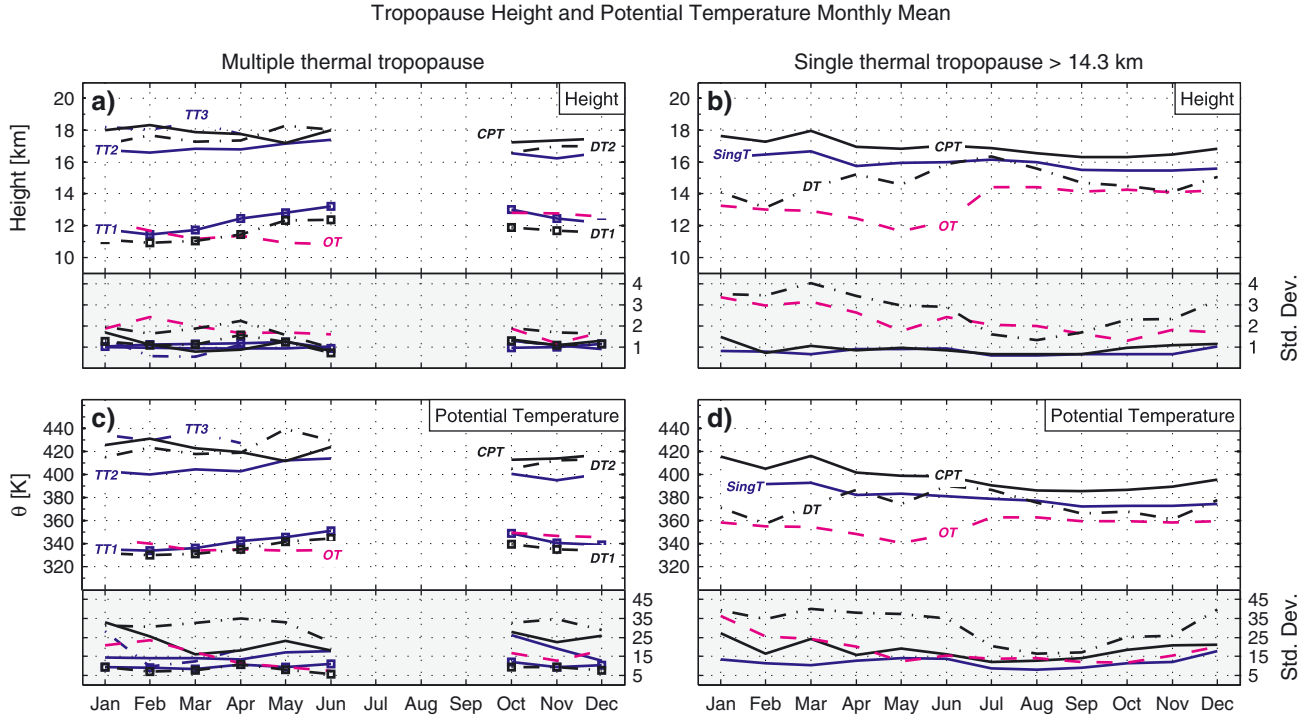

Figure 6. Monthly mean and standard deviation for (a, b) tropopause height and (c, d) potential temperature for multiple and single thermal tropopause events. The annual cycle is shown for four tropopause definitions labeled in figures as thermal tropopause (TT; blue solid line for TT1, TT2, and SingT and blue dashed line for the third thermal tropopause TT3), ozonopause (OT; magenta dashed line), cold point tropopause (CPT; black solid line), and dynamical tropopause (DT; black dashed line). The same nomenclature is used for corresponding standard deviation.

[39] The resulting annual cycles for SingT and CPT agree reasonably well with the TT2 and CPT features discussed so far in relation with multiple tropopause events. The SingT height shows a weak seasonality, with mean annual value ∼16 km. Maximum (∼16.5 km) and minimum (∼15.5 km) heights are observed in winter and early autumn, respectively. We do not observe the same seasonal cycle for SingT height as the one reported in recent studies concerning double tropopause systems. *Bischoff et al.* [2007], based on 30 years of radiosonde data, and later *Sivakumar et al.* [2011], based on 11 years of ozonesonde data, found a significant larger annual amplitude for the single thermal tropopause height. This discrepancy seems to be related to the fact that single thermal tropopauses lower and higher than 14.3 km were included by these authors into the statistics. The CPT is found, on average, on altitude levels ∼1 km higher than the thermal tropopause. Both SingT and CPT show very low variability for all the seasons, lower than ∼1 km. Annual mean values for θ_{SingT} and θ_{CPT} are ∼380 K and ∼400 K, respectively. A similar seasonal cycle to that of height is observed, with maximum in winter-spring (θ_{SingT} ∼390 K and θ_{CPT} ∼410 K) and minimum in summer-autumn (θ_{singT} ∼375 K and θ_{CPT} ∼390 K).

[40] Current definitions of the tropical TTL disagree about bottom and top bounds. *Gettelman and Forster* [2002] set the upper limit at the CPT level, while *Fueglistaler et al.* [2009] set this same limit at ∼70 hPa (425 K, 18.5 km). We found in this study that both definitions are equivalent in relation to double tropopause events whereas in the case of single tropopause events they are slightly different. A closer analysis of the vertical profiles of temperature indicates that the TT3 is located at or in the vicinity of the minimum temperature level and often related with a secondary wind speed maximum above the STJ. From this, we can conclude that the TT3 observed may be the result of enhanced poleward transport of tropical air masses near the upper bound of the tropical TTL. These results, together with the previous climatological characterization of the thermal and cold point tropopauses, provide further observational support to the tropical TTL upper limit as coincident with the definition suggested by *Fueglistaler et al.* [2009]. Additional analysis is needed to characterize and quantify the transport of tropical air masses in the subtropical UTLS and the generation of the TT3.

3.2.2. Subtropical Dynamical Tropopause

[41] It is expected the dynamical tropopause to be located in the vicinity of the thermal tropopause since the thermal tropopause itself marks the location of an abrupt transition in the concentration of atmospheric properties, including potential vorticity [*World Meteorological Organization (WMO)*, 1986]. We show in Figure 7 time-height cross sections of LPV vertical gradient for double (top) and single (bottom) thermal tropopause events, together with the annual cycle for the thermal and dynamical tropopause height (blue and black thick solid lines, respectively). Sharp positive vertical gradients are successfully assigned to the DT. Figure 7 reveals further interesting features of the subtropical UTLS which will be analyzed next.

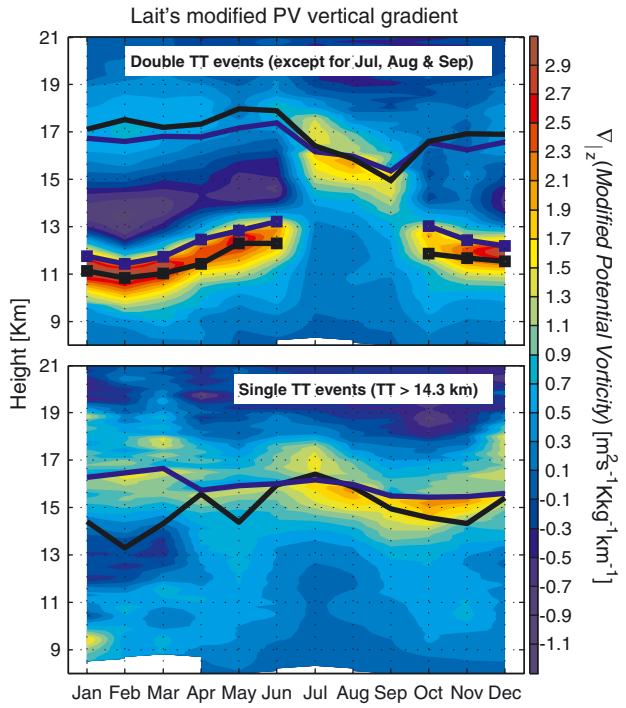

Figure 7. Time-height cross sections of Lait's modified potential vorticity vertical gradient from 8 to 21 km height for (top) double and (bottom) single thermal tropopause scenarios. Climatological values for July to August are identical in both plots. The thermal and dynamical tropopauses are shown as blue and black thick solid lines, respectively.

[42] Monthly mean DT height agrees fairly well with the corresponding values of thermal tropopause, although substantial differences are observed for both double and single thermal tropopause events. For double tropopauses (Figure 6a), a good agreement is found between both the first (TT1) and the second (TT2) thermal tropopauses and the corresponding dynamical tropopauses (DT1 and DT2, respectively). Mean altitude differences in both cases are ∼1 km, with DT1 (DT2) lower (higher) than TT1 (TT2). The calculated variability (in terms of the standard deviation) for the DT1 height is on the order of 1 km throughout the year. In the case of the DT2 height, the observed annual variability is larger, ∼1.5 km on average, with maximum during winter and early-spring (∼2 km). Potential temperature associated to DT1 and DT2 is on the order of 335 K and 420 K, respectively (see Figure 6c). The larger DT2 variability observed for both height and potential temperature in winter-spring may be related to the enhanced transport of tropical upper tropospheric air above the core of the STJ, as has been documented previously in several studies [*Haynes and Shuckburgh*, 2000b; *Randel et al.*, 2007; *Pan et al.*, 2009]. As pointed out by *Pan et al.* [2009], because of the weak gradients in the wind fields above the jet core, a main component of PV in this region should be the static stability. Since strong variations in static stability above the jet core are likely to be found depending on to what extent tropical upper troposphere air masses are being transported poleward, it is also expected large temporal variations in PV fields. Furthermore, when the STJ is located in its southernmost position, we observe the northern edge of the tropical tropopause enters deep into the midlatitude lowermost stratosphere (LMS) above our station. As the STJ moves poleward, approaching the station, the midlatitude LMS will be perturbed to a greater degree by tropical upper tropospheric air masses. This mechanism may also contribute to explain the large DT2 height variability during winter-spring.

[43] A weaker agreement between DT and SingT height is found when single thermal tropopause scenario is considered (Figure 6b). In this case the two tropopauses deviate, with the SingT at a higher altitude than the DT. An annual cycle in altitude differences is observed, with the maximum (∼2–3 km) and minimum (∼0.5 km) occurring in winter and summer, respectively. As expected, a similar annual cycle for the potential temperature is observed. A clear semiannual cycle for the annual variability of the DT height is observed, with maximum during winter and early spring (∼3 km) and minimum in summer season (∼1.5 km). It is worth noting that although similar in magnitude (∼35 K), the large winter-spring variability of the DT2 and the single DT potential temperature are different in origin. The DT2 profiles describe midlatitude LMS characteristics, where small altitude variations comprise large θ variations. In the case of the single DT profiles, the winter-spring θ standard deviation is related with larger variability of the DT height.

[44] The reasons for the above mentioned discrepancies are made clear in Figure 7. Enhanced regions of LPV vertical gradient exist in the vicinity of both DT1 and DT2, reflecting the existence of barriers to cross-tropopause transport processes. This is especially true for the DT1, while vertical gradients of LPV are weaker near the DT2, indicating a more permeable boundary between the stratosphere and the troposphere. These results are consistent with the well-known seasonal cycle of STE processes, with very little STE below the 330 K isentropic surface in the winter hemisphere and increased STE above the 340 K isentropic surface in the summer hemisphere [e.g., *Chen*, 1995]. Negative LPV vertical gradients in the intertropopause region are related with frequent occurrences of decreasing values of EPV with altitude, associated to tropical upper tropospheric air masses above the DT1. With respect to the single tropopause scheme (Figure 7, bottom), the LPV vertical gradient structure observed in the altitude range 8 to 13 km, although weaker in strength, resembles the same pattern found in relation to double tropopause scheme. The observed fingerprint of DT1 during single tropopause events might bias the corresponding DT monthly averaged height toward lower levels. We will go further on this topic in relation to the ozonopause discussion.

[45] In order to compare the LPV vertical gradient-based DT with the DT defined by a selected EPV value, we discuss next the annual cycle of DT in terms of EPV units. The DT height is defined as the altitude where a maximum in LPV vertical gradient is found. Once such level is located, we retain the corresponding EPV value. Monthly averaged EPV values associated with the dynamical tropopause in double and simple tropopause scheme are shown in Figure 8. Single tropopauses have been split into single low tropopauses ($\leq$14.3km) and single high tropopauses (>14.3km). Because of the reduced number of profiles showing single thermal tropopause height lower than 14.3 km (see Table 1), we have omitted statistics for January to March.

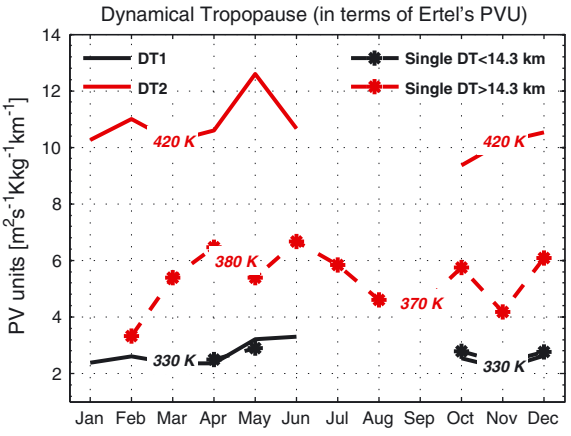

Figure 8. Ertel's PV value for the dynamical tropopause grouped into four different categories: DT higher than 14.3 km height in multiple (red solid line) and single thermal tropopause systems (red dashed line) and DT lower than 14.3 km height in multiple (black solid line) and single thermal tropopause systems (black dashed line). Data gaps during the period from January through March are due to the scarcity of profiles showing single thermal tropopause lower than 14.3 km.

[46] There are two features in the seasonal cycles shown in Figure 8 that should be emphasized. First, is the close agreement between the lower component of multiple tropopause systems and the single DT lower than 14.3 km, with annual mean around 2.5 PVU and no significant seasonality. A second remarkable feature is the contrast between DT2 and the single DT higher than 14.3 km. An EPV value ranging from 10 to 11 PVU is, on average, representative of DT2, while EPV values associated with the high single DT fall in the range 4–6 PVU, with maximum values occurring in summer and minimum in winter. Since both DT2 and single DT higher than 14.3 km were found at around 16 km height, the large differences in PVU observed suggest that air masses located at ∼16 km should have different origins depending on what type of tropopause scenario is being sampled. Low PV values (4–6 PVU) associated to the single DT higher than 14.3 km (∼380 K, see Figure 6d) indicate tropical tropospheric influence. On the contrary, high PV values (10–11 PVU) associated with DT2 (∼420 K, see Figure 6c) reveals a clear stratospheric signature, corresponding to the poleward extension of the tropical tropopause into the midlatitude LMS. We must emphasize here that a single tropopause is not the most common tropopause scheme at Tenerife site, representative of the subtropical region. It is also interesting to highlight the close agreement of our results with those reported by *Kunz et al.* [2011a] for isentropes within the 330–350 K range, but using rather different methods. Note that we analyzed in this study isentropes up to 420 K.

3.2.3. Subtropical Ozonopause

[47] The OT height exhibits greater complexity as compared to thermal and dynamical tropopauses, as can be inferred from time-height cross sections of ozone partial pressure for double (Figure 9, top) and single (Figure 9, bottom) tropopause events. With respect to multiple tropopause events, the OT is observed between 11 and 13 km (330–350 K) in good agreement with TT1/DT1, except during late spring (May and June) when it is located ∼2 km lower. Particularly noteworthy is the fact that during this period, the observed altitude differences between thermal tropopause and ozonopause do not agree with previous studies reporting an ozonopause ∼800 m lower, on average, than the thermal tropopause [*Bethan et al.*, 1996; *Schmidt et al.*, 2010]. A second ozonopause (OT2) is clearly observed at ∼17 km height, coincident with CPT, TT2, and DT2 levels (see Figure 9, top). A precise algorithm to determine analytically the OT2 exceeds the scope of this work due to implementation difficulties, as expected from the complex distribution of ozone observed in the intertropopause region.

[48] The relatively low OT heights observed from April to June in the double tropopause scheme might result of two complementary mechanisms:

[49] 1. Irreversible transport of lowermost stratospheric ozone into the upper troposphere southward of and below the STJ, associated to a still STJ [see, e.g., *Manney et al.*, 2011, and references therein]. Whenever the subtropical tropopause break, and the associated STJ, is located above or north of Tenerife, we observe equatorward intrusions of ozone-rich air from the midlatitude LMS into the subtropical upper troposphere below the STJ core, which may contribute to the lower ozonopause observed in spring. This is further supported by the fact that PVU values associated to the DT1 are slightly higher in spring (EPV > 3 PVU) than in winter (EPV ∼ 2.5 PVU), as shown in Figure 8.

[50] 2. Stratospheric intrusions associated with baroclinic instabilities occurring north of Tenerife. *Cuevas and Rodriguez* [2002] analyzed an 11 year climatology of ECMWF isentropic potential vorticity fields, reporting that the frequency of cutoff lows occurrences over the North Atlantic reaches a maximum in May-July in areas surrounding the Iberian Peninsula. *James et al.* [2003], based on a 15 year climatology of stratosphere to troposphere (STT), concluded that the corridor parallel to the Atlantic coast of the Iberian Peninsula over the ocean down to the Canaries frequently receives stratospheric air. Clear traces of stratospheric air mass intrusions exist into the upper subtropical troposphere, where relatively high ozone values below TT1 and DT1 in May and June are observed (Figure 9). The lack of agreement between OT and DT may be caused by the existence of diabatic process associated to baroclinic instabilities in the upper subtropical troposphere, weakening the good ozone-PV correlation normally observed in the absence of such processes [e.g., *Danielsen*, 1968; *Beekmann et al.*, 1994].

[51] With respect to single tropopause events (Figure 9, bottom), a semiannual cycle for the OT height is observed. From January to June, the OT is observed between 12 and 13 km (340–360 K) and differs greatly from the SingT monthly values (around 16 km; 390 K). From July to December, a very stable OT is at ∼14 km height (360 K) showing height differences with SingT and DT within 1 km.

[52] The greater altitude differences between the OT and SingT/DT occur in spring and early summer (∼4 km), which are probably due to the same atmospheric processes already addressed in relation with the double tropopause scheme. Note the similarities in monthly values of the OT height and θ during the period from April to June in both single

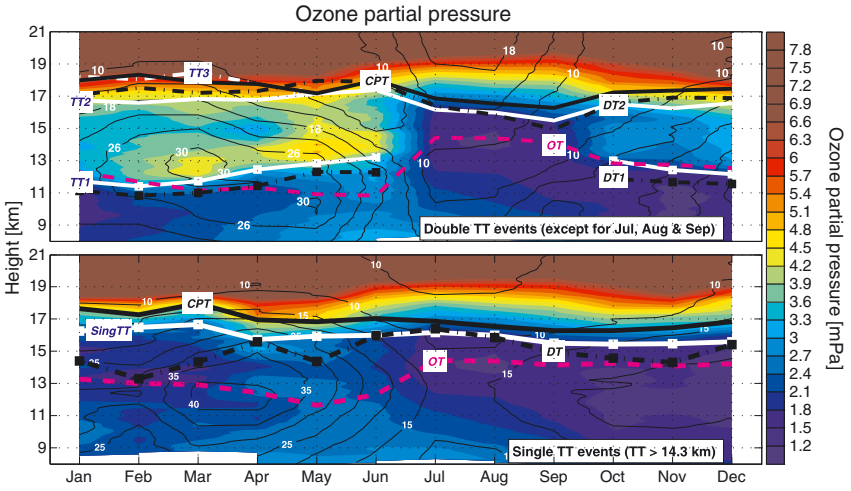

Figure 9. Time-height cross section of ozone partial pressure (mPa) and wind speed contours (m s^{-1}) from 8 to 21 km height for (top) multiple and (bottom) single thermal tropopause events. The vertical coordinate is tropopause based. The different tropopause types are shown labeled with their corresponding acronym.

and double tropopause events. Furthermore, from this, we conclude that baroclinic instabilities in the upper subtropical troposphere may play a key role in the ozone vertical distribution during this season in the subtropics.

[53] The situation is rather different in wintertime (January to March), when closer agreement between both the OT and the DT (within the statistical error) and lower altitude differences with the SingT (∼2 km) are observed. The similar variability observed for OT and DT in wintertime suggests that both tropopauses should be affected by the same atmospheric processes. The analysis of 500 hPa geopotential for each day in which is recorded a single high tropopause (>14.3 km, 36 cases) reveals that in most cases a high ridge or an Omega-shaped blocking system on the eastern North Atlantic is observed. Blocking systems, associated to a higher frequency of Rossby wave breaking processes in winter [*Wernli and Sprenger*, 2007], modify the averaged position of the STJ in this season (20°N). As a result, a stronger jet emerges northward of Tenerife, and, therefore, a tropical upper troposphere is observed above and southward of Tenerife. In a recent paper, *Manney et al.* [2011] have reported frequent excursions of a sector (or sectors) of the STJ to high latitudes in winter driven by upper tropospheric ridges and blocking system events.

[54] The significantly lower DT and OT heights (13–14 km) during January to March compared to that of the SingT (∼16 km) suggest a possible fingerprint of the DT1 and OT before the blocking system disrupts the normal upper tropospheric flow (see Figure 9). This might bias the corresponding OT and DT monthly averaged heights toward lower levels. Nevertheless, note in Figures 7 and 9 that upper DT and OT tropopauses, associated to a higher level of strong vertical ozone and LPV gradients, are detected quite close to the DT2 level observed in the double tropopause scheme.

[55] The UTLS, and more specifically the intertropopause region (between TT1 and TT2), shows sharp ozone vertical gradients, particularly during late winter and spring. Vertical distribution of ozone in this region is associated with the latitudinal position of the STJ in the vicinity of Tenerife. It is known that the core of the subtropical jet is associated with strong gradients in isentropic PV [*Chen*, 1995; *Haynes and Shuckburgh*, 2000b] and chemical tracers [*Ray et al.*, 2004]. Thus, dynamical mechanisms responsible for mixing and tracer exchange between stratosphere and troposphere occur mainly on the top and just below the jet core [*Haynes and Shuckburgh*, 2000b; *Pan et al.*, 2009]. These STE processes occurring around the STJ may explain the high variability of ozone observed in the intertropopause region. Low ozone layers occurring at around 14–15 km height (winter-spring) suggest poleward meridional transport of tropical ozone-poor air masses into the midlatitude LMS, while high ozone layers observed within 2 km above the TT1 in winter and spring are related to equatorward meridional transport of ozone-rich air masses from the midlatitude LMS. Further detailed analysis is needed to properly quantify the quasi-horizontal transport observed within the intertropopause region.

3.3. Statistics of the Subtropical Tropopause Inversion Layer

[56] In the following, we will describe the long-term mean structure and variability of the tropopause inversion layer (TIL). For the quantification of the TIL depth, we use the Brunt-Väisälä frequency squared, in a similar way as in previous studies on tropopause static stability [*Bell and Geller*, 2008; *Son et al.*, 2011]: we define the TIL depth as the vertical distance separating the maximum N^2 at the tropopause level from the altitude where N^2 is a minimum in the lower stratosphere.

[57] Figure 10 shows the seasonal cycle of the TIL depth. We have split the total number of vertical profiles available into two subgroups according to the following criteria: (1) first (or single) thermal tropopause (red boxplots) and (2) thermal tropopauses higher than 14.3 km, regardless of the thermal tropopause scenario, double or single (green boxplots). We used this criterion (i.e., first thermal tropopause detected) instead of selecting vertical profiles showing a low

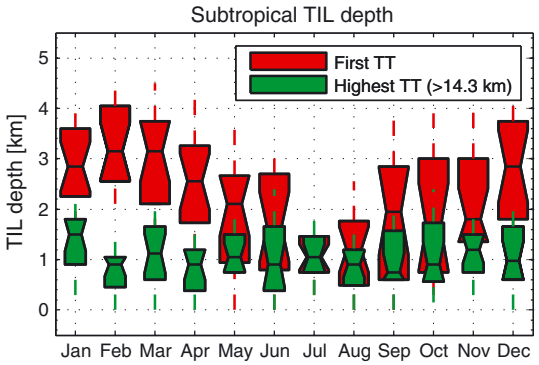

Figure 10. Notched boxplot for the TIL-depth seasonal cycle for the first (or single) thermal tropopause (red boxplots) and for thermal tropopauses higher than 14.3 km, regardless of the thermal tropopause scenario, double or single (green boxplots). Solid lines and boxes mark the median and upper and lower quartiles. All vertical profiles were tropopause level referenced.

thermal tropopause (midlatitude representative) for better comparison with results from previous analysis.

[58] As expected, these two subgroups agree during the summer season, when a single high tropopause is detected (see Table 1). For the high thermal tropopause subset, the TIL depth exhibits no significant seasonal variability with median value ∼1 km throughout the year. This occurs even when multiple tropopauses are detected (from October to June). Comparison of this result with those of recent observational studies of the global static stability field [e.g., *Bell and Geller*, 2008; *Grise et al.*, 2010] provides further evidence of the tropical character of the higher tropopause found in multiple tropopause events. The situation is more complex in the case of the first (or single) tropopause, with a clear seasonal cycle and larger dispersion in monthly means. Maximum TIL-depth values are observed during the winter season (December to March) with median values ∼3 km. The TIL is thinner during spring and autumn seasons, with median values ∼2 km and greater depth variability as compared to winter.

[59] These results support the observed extratropical TIL-depth features of previous studies [*Birner*, 2006; *Randel et al.*, 2007; *Bell and Geller*, 2008; *Schmidt et al.*, 2010]. In these studies the authors have reported a persistent TIL over the year, sharp and strong during the warmer months and deeper and weaker during the colder months. Note that nothing can be stated about the summer midlatitude TIL in this work, since we do not observe it but only the tropical tropopause. Concerning the observed TIL-depth of the first (or single) thermal tropopause during spring and autumn seasons, it is worth noting that, inherent to the criterion used for selecting the sample profiles, profiles showing single tropopause heights lower and higher than the 14.3 km threshold have been included into the same data subset. If we included tropopauses higher than 14.3 km into the statistics, that is, tropopauses with tropical signature, it would result in a net decreasing of the climatological TIL-depth values. This argument would explain the marked seasonal cycle observed in Figure 10, more evident as the number of high tropopauses included in the statistics increased. Furthermore, it also points to the selection of the proper tropopause level as a key factor in deriving reliable climatological values, especially in the latitude band from 30° to 40°, where multiple tropopause systems are likely to be found [*Añel et al.*, 2007; *Bischoff et al.*, 2007; *Randel et al.*, 2007; *Peevey et al.*, 2012].

[60] In order to obtain a precise characterization of the tropopause inversion layer of both low and high tropopauses observed at subtropics, we have applied the threshold 14.3 km to the tropopause heights. Figure 11 shows the annual cycle of static stability using tropopause-relative vertical coordinates. Note that we have readjusted the vertical coordinate by the seasonal mean tropopause height. The thick solid black line represents the tropopause height used as a reference. We have plotted mean profiles showing thermal tropopause height ≤14.3 km (Figure 11, left) and profiles showing thermal tropopause height >14.3 km (Figure 11, right). Due to the scarcity of available profiles showing low tropopause, we removed the correspondingly climatological values from July to September.

[61] Apart from the well-known sharp transition between tropospheric values ($\sim 1.0 \times 10^{-4}$ s^{-2}) and stratospheric values ($\sim 5.0 \times 10^{-4}$ s^{-2}) that occurs just at the tropopause level, the most prominent feature of the vertical N^2 section is the region within about 13–16 km in winter and early spring with reduced values of static stability $\sim 2.5 \times 10^{-4}$ s^{-2}. This is clearly related to the presence of multiple tropopause systems and the associated STJ, resulting in a mixing region with both tropical upper troposphere and midlatitude lower stratosphere characteristics [e.g., *Ray et al.*, 2004; *Pan et al.*, 2006]. Also noteworthy is the maximum in static stability observed just above the tropopause level, which is a characteristic of the TIL. Outside the region within 10–18 km, a rather small seasonality in static stability is observed, with the exception of a broad maximum $\sim 6.0 \times 10^{-4}$ s^{-2} centered at ∼19 km during the summer season (Figure 11, right). A similar maximum located above the tropical tropopause has been recently documented [*Grise et al.*, 2010; *Schmidt et al.*, 2010], but unlike *Grise et al.* [2010], we do not observe this local maximum in winter but in summer. The minimum in static stability below the tropopause is about 2–3 km lower in summer (tropical tropopause) as compared to the low tropopause observed from October to June (midlatitude tropopause).

[62] The seasonal variability of the static stability (N^2) and temperature profiles was analyzed for winter (December-January-February), spring (March-April-May), summer (June-July-August), and autumn (September-October-November) for the lower and higher tropopause (Figure 12). The vertical coordinate is centered at the thermal tropopause, and individual properties are shown for a ±6 km vertical range. This allows us to focus on the fine-scale structure of the TIL.

[63] A typical N^2 vertical structure is observed for the lower tropopause (Figure 12a), showing main characteristics in agreement with other previous studies [e.g., *Birner*, 2006; *Randel et al.*, 2007; *Bell and Geller*, 2008; *Schmidt et al.*, 2010; *Son et al.*, 2011]. The maximum values of N^2 are found nearly coincident with the tropopause, in contrast with previous results based on GPS high-resolution data reporting a maximum N^2 slightly above the tropopause for all latitudes. As suggested in *Randel et al.* [2007], this

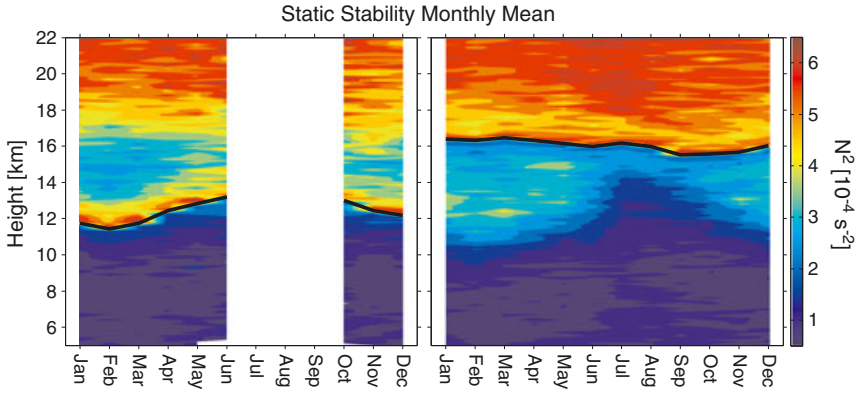

Figure 11. Annual cycle of static stability (N^2) based on two data sets grouped according to the tropopause height: (left) tropopause height lower than 14.3 km (extratropical thermal tropopause) and (right) tropopause height higher than 14.3 km (tropical thermal tropopause). The vertical coordinate is tropopause based. The thick solid black line represents the tropopause height used as a reference. White areas represent data gaps (very few single thermal tropopauses lower than 14.3 km height are observed from July to September).

discrepancy in maximum N^2 height may be related to the higher resolution of radiosondes (∼30 m) compared to GPS data (∼200 m). The maximum values of static stability are observed in winter and spring (∼ 6.0×10^{-4} s^{-2}), decreasing slightly during autumn (∼ 5.0×10^{-4} s^{-2}). A similar seasonality is observed in the TIL depth, varying between maximum ∼3 km in winter and spring, and ∼2 km during autumn. In contrast, the minimum N^2 value above the tropopause level is found to be approximately constant (∼ 3.0×10^{-4} s^{-2}). These results agree with what *Birner* [2006] has called the summer-winter contrast, referring to the distinct properties of the TIL between winter and summer (deeper and more clearly defined during the cold season), and further confirmed in later investigations [*Bell and Geller*, 2008; *Schmidt et al.*, 2010]. There are no substantial seasonal differences in static stability below the tropopause, with a near-discontinuity in N^2 gradient at ∼2–3 km for all the mean profiles.

[64] Figure 12b shows the N^2 vertical structure for the higher tropopause (the corresponding temperature profiles are shown in Figure 12d). The results obtained in this case are especially valuable as very few investigations have been conducted on tropical TIL, with the exception of recent global coverage analysis of static stability in the stratosphere and upper troposphere [e.g., *Grise et al.*, 2010]. In contrast to the previous discussion, there is no difference between the maximum N^2 in winter and summer, with mean value below 6.0×10^{-4} s^{-2} all the year round, and nearly coincident with the tropopause. The TIL depth is almost constant (∼1 km) throughout the year whereas the minimum N^2 value above the tropopause shows little variation with season, with mean value ∼ 4.5×10^{-4} s^{-2}. As discussed before, a weak signature of a secondary maximum in static stability near 3 km above the tropopause is observed during summer. The greater seasonal variability in static stability occurs below the tropopause. Nevertheless, it should be noted that mean profiles corresponding to winter and spring are highly perturbed below the tropopause by the presence of multiple tropopause systems and the associated STJ, and thus they should not be representative of the tropical upper

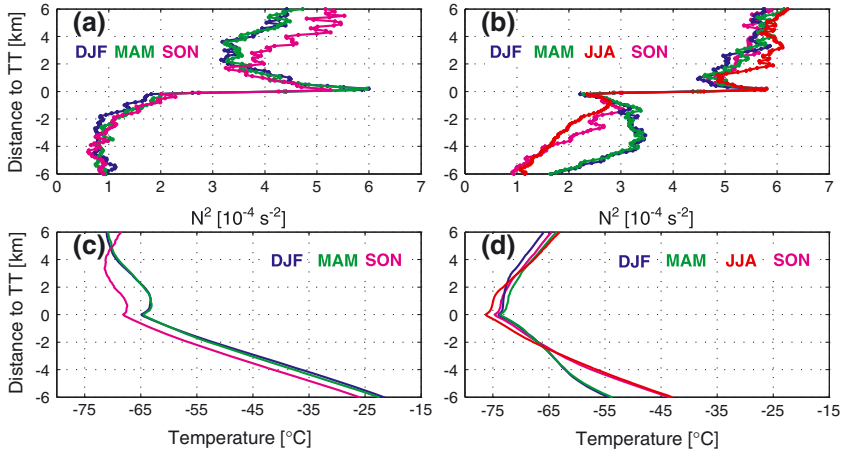

Figure 12. Seasonal mean N^2 and temperature profiles based on two data sets grouped according to the tropopause height: (a, c) tropopause height lower than 14.3 km and (b, d) tropopause height higher than 14.3 km. The vertical coordinate is tropopause based.

troposphere. Despite this, it is notable of the reduced static stability from ∼1 km below the tropopause, regardless of the season. This is found to be an exclusive feature of the tropical tropopause, which furthermore agrees with the height of the so-called zero radiative heating level in relation to the tropical tropopause transition layer radiative balance [see, e.g., *Gettelman et al.*, 2004, and references therein].

4. Summary and Concluding Remarks

[65] In this paper we have examined the structure of the subtropical UTLS region on the basis of 20 years of highly resolved ozonesonde and ECMWF ERA-Interim potential vorticity and zonal wind vertical profiles data. The Izaña Atmospheric Research Center (Tenerife; 28°N, 16°W) is located at a subtropical site characterized by frequent multiple tropopause events (subtropical tropopause-break) associated to the STJ. The primary goal of this work was to obtain further knowledge and understanding of the subtropical UTLS, especially when model reanalysis is not able to adequately resolve the observed fine structures of this singular atmospheric region [*Reichler et al.*, 2003; *Bell and Geller*, 2008; *Homeyer et al.*, 2010; *Son et al.*, 2011]. The results obtained in this study are expected to be comparable to those obtained at any other location in the subtropical belt under similar upper tropospheric flow conditions.

[66] The subtropical UTLS is revealed as a complex atmospheric region with a thickness ∼8 km, which is characterized by the analysis and evaluation of four different tropopause definitions: lapse rate (thermal), cold point, ozone, and dynamical tropopauses. Climatologies of tropopause height, potential vorticity, and potential temperature were produced for the period November 1992 to December 2011. The seasonal cycle of multiple tropopauses was calculated including percentage of first, second, and third thermal tropopauses observed. The results obtained were briefly discussed on the basis of the averaged STJ position relative to the station. From this analysis we concluded that the threshold height 14.3 km is suitable to discriminate air masses with tropical characteristics (thermal tropopause > 14.3 km) from those with extratropical characteristics (thermal tropopause < 14.3 km). We have then focused on describing the observational differences between multiple and single tropopause events, including detailed analyses of ozone and Lait's modified PV vertical gradient structures in the subtropical UTLS. When dealing with single tropopause events, we removed from the data set all those soundings for which the thermal tropopause was found to be lower than 14.3 km, since there were very few soundings with tropopause heights lower than this threshold. We avoid in this way mixing air masses with rather different characteristics. In addition, we have investigated the long-term mean structure and variability of the tropopause inversion layer using N^2 profiles representative of tropical and midlatitude air masses.

[67] The main results of this paper are the following:

[68] 1. The frequency occurrence of multiple tropopauses is maximum in winter (∼80%) and minimum in summer (< 5%). We observed transition periods in April–June (September–November) with decreasing (increasing) occurrences of multiple tropopauses, closely related to the STJ position relative to the station. These observations agreed well with the knowledge that double tropopauses are preferably found at and poleward of the STJ [*Schmidt et al.*, 2006; *Castanheira and Gimeno*, 2011; *Peevey et al.*, 2012]. We suggest as a possible cause for the occurrence of multiple (more than two) thermal tropopauses the enhanced poleward transport of tropical air masses near the upper bound of the tropical TTL.

[69] 2. The climatological values of tropopause height and potential temperature are similar to previous studies based on radiosonde [*Seidel et al.*, 2001; *Gettelman and Forster*, 2002; *Bischoff et al.*, 2007; *Sivakumar et al.*, 2011] and satellite [*Kishore et al.*, 2006; *Son et al.*, 2011] data. However, as concerns single tropopause events, there are significant differences between our results and tropopause heights reported by *Bischoff et al.* [2007] and *Sivakumar et al.* [2011], probably due to the fact that these authors have averaged tropopause height without previously separating high from low tropopauses. The CPT and the TT3 are found at levels well close each other, ∼18.5 km (∼425 K), in agreement with the tropical TTL upper limit as suggested by *Fueglistaler et al.* [2009].

[70] 3. We have presented in this paper a novel method to determine the dynamical tropopause based on the vertical gradient of Lait's modified PV (LPV) which is substantially different to that developed in a recent study by *Kunz et al.* [2011a]. Nevertheless, the proposed approach may have difficulties in the near vicinity of jets, where PV isopleths distortions are expected to modify LPV vertical gradients. Ertel's PV values associated to the dynamical tropopause correspond well with those found by *Kunz et al.* [2011a] for isentropes within the 310–350 K range.

[71] 4. A second dynamical tropopause (DT2) has been introduced in this paper which, to the authors' knowledge, represents a novel concept in the literature. The DT2 height and potential temperature have been characterized throughout the year, showing a fairly good agreement with the TT2. The DT2 corresponds also to a sharp ozone vertical gradient, suggesting the existence of a second ozonopause (OT2). The OT2 has been identified in this study although its analytical determination constitutes a complex task which exceeds the scope of the current study.

[72] 5. We found a good agreement between OT and DT except in spring when the OT is located at significant lower levels (altitude differences ∼2 km) regardless of whether multiple or single tropopause events were considered. We proposed stratospheric intrusions associated with baroclinic instabilities occurring north of Tenerife, very frequent during this season [*Cuevas and Rodriguez*, 2002; *James et al.*, 2003], as the main mechanism responsible of the lower OT observed in spring. Furthermore, baroclinic instabilities in the upper subtropical troposphere, and the diabatic processes associated, also provide an explanation to the lack of agreement between OT and DT in spring. Indeed, the existence of such processes may result in weaker ozone-PV correlation [e.g., *Danielsen* [1968] and *Beekmann et al.* [1994]]. A key feature of the subtropical UTLS, resulting from frequent poleward transport of tropical tropospheric air above the STJ, is the region within about 13–16 km in winter and early spring, with notably reduced values of static stability and sharp ozone and PV vertical gradients.

[73] 6. Altitude differences between TT, on the one hand, and DT and OT, on the other, are found to be on average

∼1 km except for soundings corresponding to a single thermal tropopause >14.3 km, when maximum differences (∼2–3 km) are observed in winter. A clear fingerprint of DT1 and OT observed during these events in winter-autumn might result in significant bias toward lower levels in DT and OT monthly averaged height. We suggest that the observed signature of DT1 and OT should be originated in the frequent occurrence of rapidly evolving blocking systems during winter which resulted in a stronger jet shifted well north of its usual winter position.

[74] 7. The tropical TIL shows little seasonal variability and is found to be thinner (∼1 km) than the midlatitude counterpart, in agreement with previous studies. It is notable of the reduced static stability (N^2) from ∼1 km below the tropopause, regardless of the season. This is found to be an exclusive feature of the tropical tropopause, which furthermore agrees with the height of the so-called zero radiative heating level in relation to the tropical TTL radiative balance [*Gettelman et al.*, 2004]. This provides a method to unambiguously distinguish the tropical from the midlatitude tropopause. The midlatitude thermal tropopause shows a clear annual cycle, with maximum TIL depth during winter (∼3 km).

[75] 8. Ozone-rich and high static stability layers of ∼2 km thickness above the TT1 and an ∼2 km thick layer with strong LPV vertical gradients below it indicate that the TT1 represents a strong barrier to cross-tropopause transport. This implies that on a climatological basis, as pointed out by *Birner* [2006], quasi-horizontal mixing along isentropes is the main transport process in the tropopause region. Significant differences in enhanced LPV vertical gradient structures associated to the higher dynamical tropopause suggest that the tropical tropopause might be more permeable to cross-tropopause transport. A key feature of the subtropical UTLS, resulting from frequent poleward transport of tropical tropospheric air above the STJ, is the region within about 13–16 km in winter and early spring with notably reduced values of static stability and sharp ozone and PV vertical gradients.

[76] **Acknowledgments.** The authors are grateful to the Izaña Atmospheric Research Center (AEMET) team in charge of the ozonesonde operations, and especially Sergio Afonso, the expert technician of ozonesonde program, and Ramon Ramos, the Izaña's field manager. Juanjo Bustos has kindly computed the PV vertical profiles from the ECMWF ERA-Interim reanalysis. We also thank Celia Milford for helpful comments during the preparation of the manuscript. The authors are grateful for the constructive comments of three anonymous reviewers.

References

Añel, J. A., J. C. Antuña, L. de la Torre, R. Nieto, and L. Gimeno (2007), Global statistics of multiple tropopauses from the IGRA database, *Geophys. Res. Lett.*, *34*(6), L06709, doi:10.1029/2006GL029224.

Assmann, R. (1902), *Über die Existenz eines wärmeren Luftstromes in der Höhe von 10 bis 15km*, 24, Sitzber. Königl. Preuss. Akad. Wiss., Berlin.

Atticks, M. G., and G. D. Robinson (1983), Some features of the structure of the tropical tropopause, *Quart. J. Roy. Meteor. Soc.*, *109*, 295–308, doi:10.1002/qj.49710946004.

Beekmann, M., G. Ancellet, and G. Mégie (1994), Climatology of tropospheric ozone in southern europe and its relation to potential vorticity, *J. Geophys. Res.*, *99*(D6), 12,841–12,853, doi:10.1029/94JD00228.

Bell, S. W., and M. A. Geller (2008), Tropopause inversion layer: Seasonal and latitudinal variations and representation in standard radiosonde data and global models, *J. Geophys. Res.*, *113*, D05109, doi:10.1029/2007JD009022.

Bethan, S., G. Vaughan, and S. J. Reid (1996), A comparison of ozone and thermal tropopause heights and the impact of tropopause definition on quantifying the ozone content of the troposphere, *Quart. J. Roy. Meteor. Soc.*, *122*(532), 929–944, doi:10.1002/qj.49712253207.

Birner, T. (2006), Fine-scale structure of the extratropical tropopause region, *J. Geophys. Res.*, *111*, D04104, doi:10.1029/2005JD006301.

Birner, T. (2010), Residual circulation and tropopause structure, *J. Atmos. Sci.*, *67*(8), 2582–2600, doi:10.1175/2010JAS3287.1.

Birner, T., A. Drnbrack, and U. Schumann (2002), How sharp is the tropopause at midlatitudes?, *Geophys. Res. Lett.*, *29*(14), 451–454, doi:10.1029/2002GL015142.

Bischoff, S. A., P. O. Canziani, and A. E. Yuchechen (2007), The tropopause at southern extratropical latitudes: Argentine operational rawinsonde climatology, *Int. J. Climatol.*, *27*(2), 189–209, doi:10.1002/joc.1385.

Castanheira, J., T. Peevey, C. Marques, and M. Olsen (2012), Relationships between Brewer-Dobson circulation, double tropopauses, ozone and stratospheric water vapour, *Atmos. Chem. Phys.*, *12*(21), 10,195–10,208, doi:10.5194/acp-12-10195-2012.

Castanheira, J. M., and L. Gimeno (2011), Association of double tropopause events with baroclinic waves, *J. Geophys. Res.*, *116*, D19113, doi:10.1029/2011JD016163.

Chawla, S., and P. Sun (2006), SLOM: A new measure for local spatial outliers, *Knowl. Inf. Syst.*, *9*(4), 412–429, doi:10.1007/s10115-005-0200-2.

Chen, P. (1995), Isentropic cross-tropopause mass exchange in the extratropics, *J. Geophys. Res.*, *100*(D8), 16,661–16,673, doi:10.1029/95JD01264.

Cuevas, E., and J. Rodriguez (eds.) (2002), *Statistics of Cutoff Lows Over the North Atlantic, Tercera Asamblea Hispano-Portuguesa de Geodesia y Geofsica*, 1–3, Valencia, Spain, 4-8 February, 2002, Comisin Española de Geodesia y Geofisica, Editorial UPV, Valencia, Spain.

Cuevas, E., K. Lamb, and Bais A. (1994), *Total Ozone Contents Derived by Different Instruments and Soundings*, 105–119, Meteorological Publications No 27, Finnish Meteorological Institute, Helsinki.

Cuevas, E., J. Rodriguez, and J. Bustos (eds.) (1999), *A preliminary statistics of the subtropical jet during 1998, 2nd TRACAS European Project meeting*, Annual Report of the TRACAS European Project, Puerto de la Cruz (S/C de Tenerife), 21–22 January.

Danielsen, E. F. (1968), Stratospheric-tropospheric exchange based on radioactivity, ozone and potential vorticity, *J. Atmos. Sci.*, *25*(3), 502–518.

Ertel, H. (1942), Ein neuer hydrodynamischer wirbelsatz, *Meteor. Z*, *59*, 271–281.

Fueglistaler, S., A. E. Dessler, T. J. Dunkerton, I. Folkins, Q. Fu, and P. W. Mote (2009), Tropical tropopause layer, *Rev. Geophys.*, *47*, RG1004, doi:10.1029/2008RG000267.

Gettelman, A., and T. Birner (2007), Insights into tropical tropopause layer processes using global models, *J. Geophys. Res.*, *112*, D23104, doi:10.1029/2007JD008945.

Gettelman, A., and P. Forster (2002), A climatology of the tropical tropopause layer, *J. Meteorol. Soc. Jpn.*, *80*(4B), 911–924, doi:10.2151/jmsj.80.911.

Gettelman, A., P. M. d. Forster, M. Fujiwara, Q. Fu, H. Vömel, L. K. Gohar, C. Johanson, and M. Ammerman (2004), Radiation balance of the tropical tropopause layer, *J. Geophys. Res.*, *109*, D07103, doi:10.1029/2003JD004190.

Gettelman, A., P. Hoor, L. L. Pan, W. J. Randel, M. I. Hegglin, and T. Birner (2011), The extratropical upper troposphere and lower stratosphere, *Rev. Geophys.*, *49*, RG3003, doi:10.1029/2011RG000355.

Grise, K. M., D. W. J. Thompson, and T. Birner (2010), A global survey of static stability in the stratosphere and upper troposphere, *J. Climate*, *23*, 2275–2292, doi:10.1175/2009JCLI3369.1.

Haynes, P., and E. Shuckburgh (2000b), Effective diffusivity as a diagnostic of atmospheric transport: 2. Troposphere and lower stratosphere, *J. Geophys. Res.*, *105*(D18), 22,795–22,810, doi:10.1029/2000JD900092.

Haynes, P., J. Scinocca, and M. Greenslade (2001), Formation and maintenance of the extratropical tropopause by baroclinic eddies, *Geophys. Res. Lett.*, *28*(22), 4179–4182, doi:10.1029/2001GL013485.

Hegglin, M. I., C. D. Boone, G. L. Manney, and K. A. Walker (2009), A global view of the extratropical tropopause transition layer from atmospheric chemistry experiment Fourier transform spectrometer O_3, H_2O, and CO, *J. Geophys. Res.*, *114*, D00B11, doi:10.1029/2008JD009984.

Highwood, E. J., and B. J. Hoskins (1998), The tropical tropopause, *Quart. J. Roy. Meteor. Soc.*, *124*(549), 1579–1604, doi:10.1002/qj.49712454911.

Hoerling, M. P., T. K. Schaack, and A. J. Lenzen (1991), Global objective tropopause analysis, *Mon. Wea. Rev.*, *119*(8), 1816–1831.

Hoinka, K. (1997), The tropopause: Discovery, definition and demarcation, *Meteorol. Z. Berlin*, *6*, 281–303.

Hoinka, K. P. (1998), Statistics of the global tropopause pressure, *Mon. Wea. Rev.*, *126*(12), 3303–3325.

Holton, J. R., P. H. Haynes, M. E. McIntyre, A. R. Douglass, R. B. Rood, and L. Pfister (1995), Stratosphere-troposphere exchange, *Rev. Geophys.*, *33*(4), 403–439, doi:10.1029/95RG02097.

Homeyer, C. R., K. P. Bowman, and L. L. Pan (2010), Extratropical tropopause transition layer characteristics from high-resolution sounding data, *J. Geophys. Res.*, *115*, D13108, doi:10.1029/2009JD013664.

Hoor, P., H. Fischer, L. Lange, J. Lelieveld, and D. Brunner (2002), Seasonal variations of a mixing layer in the lowermost stratosphere as identified by the CO-O_3 correlation from in situ measurements, *J. Geophys. Res.*, *107*(D5), ACL 1-1–ACL 1-11, doi:10.1029/2000JD000289.

James, P., A. Stohl, C. Forster, S. Eckhardt, P. Seibert, and A. Frank (2003), A 15-year climatology of stratosphere–troposphere exchange with a Lagrangian particle dispersion model 2. Mean climate and seasonal variability, *J. Geophys. Res.*, *108*(D12), 8522, doi:10.1029/2002JD002639.

Kahya, C., D. Demirhan, S. Topcu, and S. Incecik (2005), An examination of the laminae characteristics in ozone profiles in eastern and south eastern Europe, *Int. J. Remote Sens.*, *26*(16), 3455–3466, doi:10.1080/01431160500076517.

Keyser, D., and M. A. Shapiro (1986), A review of the structure and dynamics of upper-level frontal zones, *Mon. Wea. Rev.*, *114*(2), 452–499.

Kishore, P., S. P. Namboothiri, K. Igarashi, J. H. Jiang, C. O. Ao, and L. J. Romans (2006), Climatological characteristics of the tropopause parameters derived from GPS/CHAMP and GPS/SAC-C measurements, *J. Geophys. Res.*, *111*(D20), D20110, doi:10.1029/2005JD006827.

Kochanski, A. (1955), Cross sections of the mean zonal flow and temperature along 80°W, *J. Meteor.*, *12*(2), 95–106.

Komhyr, W. D. (1969), Electrochemical concentration cells for gas analysis, *Ann. Geophys.*, *25*, 203–210.

Kunz, A., P. Konopka, R. Mller, L. L. Pan, C. Schiller, and F. Rohrer (2009), High static stability in the mixing layer above the extratropical tropopause, *J. Geophys. Res.*, *114*, D16305, doi:10.1029/2009JD011840.

Kunz, A., P. Konopka, R. Müller, and L. Pan (2011a), Dynamical tropopause based on isentropic potential vorticity gradients, *J. Geophys. Res.*, *116*, D01110, doi:10.1029/2010JD014343.

Kunz, A., L. Pan, P. Konopka, D. Kinnison, and S. Tilmes (2011b), Chemical and dynamical discontinuity at the extratropical tropopause based on START08 and WACCM analyses, *J. Geophys. Res.*, *116*, D24302, doi:10.1029/2011JD016686.

Lait, L. R. (1994), An alternative form for potential vorticity, *J. Atmos. Sci.*, *51*(12), 1754–1759.

Logan, J. A. (1999), An analysis of ozonesonde data for the troposphere: Recommendations for testing 3-D models and development of a gridded climatology for tropospheric ozone, *J. Geophys. Res.*, *104*(D13), 16,115–16,149, doi:10.1029/1998JD100096.

Manney, G., et al. (2011), Jet characterization in the upper troposphere/lower stratosphere (UTLS): Applications to climatology and transport studies, *Atmos. Chem. Phys.*, *11*(12), 6115–6137, doi:10.5194/acp-11-6115-2011.

Mote, P. W., K. H. Rosenlof, M. E. McIntyre, E. S. Carr, J. C. Gille, J. R. Holton, J. S. Kinnersley, H. C. Pumphrey, J. M. Russell, and J. W. Waters (1996), An atmospheric tape recorder: The imprint of tropical tropopause temperatures on stratospheric water vapor, *J. Geophys. Res.*, *101*(D2), 3989–4006, doi:10.1029/95JD03422.

Pan, L. L., W. J. Randel, B. L. Gary, M. J. Mahoney, and E. J. Hintsa (2004), Definitions and sharpness of the extratropical tropopause: A trace gas perspective, *J. Geophys. Res.*, *109*, D23103, doi:10.1029/2004JD004982.

Pan, L. L., P. Konopka, and E. V. Browell (2006), Observations and model simulations of mixing near the extratropical tropopause, *J. Geophys. Res.*, *111*, D05106, doi:10.1029/2005JD006480.

Pan, L. L., W. J. Randel, J. C. Gille, W. D. Hall, B. Nardi, S. Massie, V. Yudin, R. Khosravi, P. Konopka, and D. Tarasick (2009), Tropospheric intrusions associated with the secondary tropopause, *J. Geophys. Res.*, *114*, D10302, doi:10.1029/2008JD011374.

Peevey, T. R., J. C. Gille, C. E. Randall, and A. Kunz (2012), Investigation of double tropopause spatial and temporal global variability utilizing high resolution dynamics limb sounder temperature observations, *J. Geophys. Res.*, *117*, D01105, doi:10.1029/2011JD016443.

Randel, W. J., F. Wu, and P. Forster (2007), The extratropical tropopause inversion layer: Global observations with GPS data, and a radiative forcing mechanism, *J. Atmos. Sci.*, *64*(12), 4489–4496, doi:10.1175/2007JAS2412.1.

Ray, E. A., K. H. Rosenlof, E. Richard, D. Parrish, and R. Jakoubek (2004), Distributions of ozone in the region of the subtropical jet: An analysis of in situ aircraft measurements, *J. Geophys. Res.*, *109*, D08106, doi:10.1029/2003JD004143.

Reed, R. J. (1955), A study of a characteristic type of upper-level frontogenesis, *J. Meteor.*, *12*, 226–237.

Reichler, T., M. Dameris, and R. Sausen (2003), Determining the tropopause height from gridded data, *Geophys. Res. Lett.*, *30*(20), 2042, doi:10.1029/2003GL018240.

Rex, D. F. (1969), *Climate of the Free Atmosphere, World Survey of Climatology,* vol. 4, 450 pp., Elsevier, New York.

Rossby, C.-G. (1940), Planetary flow patterns in the atmosphere, *Quart. J. Roy. Meteor. Soc.*, *66*, 68–87.

Santer, B. D., et al. (2003), Contributions of anthropogenic and natural forcing to recent tropopause height changes, *Science*, *301*(5632), 479–483, doi:10.1126/science.1084123.

Sausen, R., and B. D. Santer (2003), Use of changes in tropopause height to detect human influences on climate, *Meteor. Z.*, *12*(3), 131–136, doi:10.1127/0941-2948/2003/0012-0131.

Schmidt, T., G. Beyerle, S. Heise, J. Wickert, and M. Rothacher (2006), A climatology of multiple tropopauses derived from GPS radio occultations with CHAMP and SAC-C, *Geophys. Res. Lett.*, *33*, L04808, doi:10.1029/2005GL024600.

Schmidt, T., J.-P. Cammas, H. G. J. Smit, S. Heise, J. Wickert, and A. Haser (2010), Observational characteristics of the tropopause inversion layer derived from CHAMP/GRACe radio occultations and MOZAIC aircraft data, *J. Geophys. Res.*, *115*, D24304, doi:10.1029/2010JD014284.

Schneider, T. (2004), The tropopause and the thermal stratification in the extratropics of a dry atmosphere, *J. Atmos. Sci.*, *61*, 1317–1340.

Seidel, D. J., R. Ross, J. K. Angell, and G. C. Reid (2001), Climatological characteristics of the tropical tropopause as revealed by radiosondes, *J. Geophys. Res.*, *106*(D8), 7857–7878, doi:10.1029/2000JD900837.

Shapiro, M. (1978), Further evidence of the mesoscale and turbulent structure of upper level jet stream frontal zone systems, *Mon. Wea. Rev.*, *106*, 1100–1111.

Sivakumar, V., J.-L. Baray, S. Baldy, and H. Bencherif (2006), Tropopause characteristics over a southern subtropical site, reunion island (21°S, 55°E): Using radiosonde-ozonesonde data, *J. Geophys. Res.*, *111*, D19111, doi:10.1029/2005JD006430.

Sivakumar, V., H. Bencherif, N. Begue, and A. M. Thompson (2011), Tropopause characteristics and variability from 11 yr of SHADOZ observations in the southern tropics and subtropics, *J. Appl. Meteor. Climatol.*, *50*(7), 1403–1416, doi:10.1175/2011JAMC2453.1.

Son, S.-W., and L. M. Polvani (2007), Dynamical formation of an extra-tropical tropopause inversion layer in a relatively simple general circulation model, *Geophys. Res. Lett.*, *34*, L17806, doi:10.1029/2007GL030564.

Son, S.-W., N. F. Tandon, and L. M. Polvani (2011), The fine-scale structure of the global tropopause derived from cosmic GPS radio occultation measurements, *J. Geophys. Res.*, *116*, D20113, doi:10.1029/2011JD016030.

Steinbrecht, W., H. Claude, U. Köhler, and K. Hoinka (1998), Correlations between tropopause height and total ozone: Implications for long-term changes, *J. Geophys. Res.*, *103*(D15), 19,183–19,192, doi:10.1029/98JD01929.

Teisserenc de Bort, L. (1902), Variations de la température de lair libre dans la zona comprise entre 8km et 13km d'altitude, *Compres Rendus de l'Acad. Sci. Paris*, *134*, 987–989.

Thuburn, J., and G. C. Craig (1997), GCM tests of theories for the height of the tropopause, *J. Atmos. Sci.*, *54*(7), 869–882.

Varotsos, C., C. Cartalis, A. Vlamakis, C. Tzanis, and I. Keramitsoglou (2004), The long-term coupling between column ozone and tropopause properties, *J. Climate*, *17*(19), 3843–3854.

Wernli, H., and M. Sprenger (2007), Identification and ERA-15 climatology of potential vorticity streamers and cutoffs near the extratropical tropopause, *J. Atmos. Sci.*, *64*(5), 1569–1586.

Wirth, V. (2001), Cyclone-anticyclone asymmetry concerning the height of the thermal and the dynamical tropopause, *J. Atmos. Sci.*, *58*(1), 26–37.

Wirth, V. (2003), Static stability in the extratropical tropopause region, *J. Atmos. Sci.*, *60*(11), 1395–1409.

Wirth, V. (2004), A dynamical mechanism for tropopause sharpening, *Meteor. Z.*, *13*(6), 477–484.

World Meteorological Organization (WMO) (1957), Meteorology—A three-dimensional science: Second session of the commission for aerology, *WMO Bull.*, *4*, 134–138.

World Meteorological Organization (WMO), (1986), Atmospheric ozone 1985: Global ozone research and monitoring project rep., *Rep. No. 16*, 392 pp, WMO, Geneva, Switzerland.

Zahn, A., et al. (2004), Passenger aircraft project CARIBIC 1997–2002, part I: The extratropical chemical tropopause, *Atmos. Chem. Phys. Discuss.*, *4*(1), 1091–1117.

Zhou, X. L., M. A. Geller, and M. H. Zhang (2001), Tropical cold point tropopause characteristics derived from ECMWF reanalyses and soundings, *J. Climate*, *14*(8), 1823–1838.